Prostaglandin E_2 synchronizes lunar-regulated beach-spawning in grass puffers

Junfeng Chen[1,2]†, Yuma Katada[1,2]†, Kousuke Okimura[1,2]†, Taiki Yamaguchi[1,2]†, Ying-Jey Guh[1,2]‡, Tomoya Nakayama[2,3], Michiyo Maruyama[1,2], Yuko Furukawa[1,2], Yusuke Nakane[1,2], Naoyuki Yamamoto[4], Yoshikatsu Sato[1], Hironori Ando[5], Asako Sugimura[6], Kazufumi Tabata[6], Ayato Sato[1], and Takashi Yoshimura[1,2,7*]

[1]Institute of Transformative Bio-Molecules (WPI-ITbM), Nagoya University, Furo-cho, Chikusa-ku, Nagoya, Aichi, 464-8601, Japan

[2]Laboratory of Animal Integrative Physiology, Graduate School of Bioagricultural Sciences, Nagoya University, Furo-cho, Chikusa-ku, Nagoya, Aichi, 464-8601, Japan

[3]Institute for Advanced Research, Nagoya University, Nagoya, Aichi, 464-8601, Japan

[4]Laboratory of Fish Biology, Graduate School of Bioagricultural Sciences, Nagoya University, Furo-cho, Chikusa-ku, Nagoya, Aichi, 464-8601, Japan

[5]Sado Marine Biological Station, Sado Island Center for Ecological Sustainability, Niigata University, 87 Tassha, Sado, Niigata, 952-2135, Japan

[6]Toyota Boshoku Corporation, 1-1 Toyoda-cho, Kariya-shi, Aichi, 448-8651, Japan

[7]Lead contact

†These authors contributed equally to this work.

‡Present address: Marine Research Station, Institute of Cellular and Organismic Biology, Academia Sinica, Jiaoxi Township, Yilan County, 262002, Taiwan

*Correspondence: takashiy@agr.nagoya-u.ac.jp

Takashi Yoshimura, Ph.D., FRSB

Institute of Transformative Bio-Molecules (WPI-ITbM)

& Graduate School of Bioagricultural Sciences

Nagoya University

Furo-cho, Chikusa-ku, Nagoya, Aichi, 464-8601, Japan

Summary

Many organisms living along the coastlines synchronize their reproduction with the lunar cycle. At the time of spring tide, thousands of grass puffers (*Takifugu alboplumbeus*) aggregate and vigorously tremble their bodies at the water's edge to spawn. To understand the mechanisms underlying this spectacular semilunar beach-spawning, we collected the hypothalamus and pituitary from male grass puffers every week for two months. RNA-sequencing (RNA-seq) analysis identified 125 semilunar genes, including genes crucial for reproduction (e.g., gonadotropin-releasing hormone 1 (*gnrh1*) and luteinizing hormone β subunit (*lhb*)) and receptors for pheromone prostaglandin E (PGE). PGE_2 is secreted into the seawater during the spawning and its administration activates olfactory sensory neurons and triggers trembling behavior of surrounding individuals. These results suggest that PGE_2 synchronizes lunar-regulated beach-spawning behavior in grass puffers. To further explore the mechanism that regulates the lunar-synchronized transcription of semilunar genes, we searched for semilunar transcription factors. Spatial transcriptomics and multiplex fluorescent *in situ* hybridization showed co-localization of the semilunar transcription factor CCAAT/enhancer-binding protein δ (*cebpd*) and *gnrh1,* and cebpd induced the promoter activity of *gnrh1*. Taken together, our study demonstrates semilunar genes that mediate lunar-synchronized beach-spawning behavior.

Keywords

lunar cycle, spring tide, neap tide, semilunar rhythm, seasonal reproduction, grass puffer, biological clock, pheromone, beach-spawning

Introduction

The highest tidal excursions, observed every two weeks at the new and full moons, are called the spring tide. Many organisms living around coastlines, such as corals, worms, insects and fish, synchronize their reproduction with the lunar cycle [1, 2]. Several studies have been performed to understand the mechanisms of lunar rhythms in the past decades. For instance, the presence of blue-light-sensing photoreceptors, cryptochromes for moonlight detection is reported in the reef-building coral [3]. A recent study on marine bristle worm reported that interpretation of moonlight is mediated by the interplay of two light sensors, cryptochrome and melanopsin ortholog [4]. The genome of a marine midge whose reproduction is timed by the circadian and circalunar clocks has been sequenced and modulation of alternative splicing is suggested to be the mechanism for natural adaptation in circadian timing [5]. However, underlying molecular mechanisms of lunar controlled rhythms are still largely obscure [1].

Beach-spawning is a large mating aggregation of fish that are synchronized to a specific time, typically occurring around high tide during the spring tides at specific sites along the shoreline. The best examples of beach-spawning fish are the grass puffer (*Takifugu alboplumbeus*) and grunion (*Leuresthes tenuis*) [6, 7]. Around the new and full moons, thousands of grass puffers aggregate in the surf zone to spawn [6, 8, 9, 10]. During the rising tide, they vigorously flop and tremble their bodies at the water's edge (Figure 1A). The dramatic sight of fish spawning has evoked great interest. In the present study, we aimed to uncover its underlying molecular mechanism.

Results

Male grass puffers are semilunar spawners

77 Female grass puffers typically spawn once a year, whereas males spawn repeatedly
78 around the spring tide during their breeding season (i.e., from mid-May to mid-July).
79 Hence, male grass puffers are semilunar spawners and an excellent model for
80 understanding lunar-regulated rhythmicity. In this study, we obtained wild male grass
81 puffers at their spawning site in Minamichita, Japan every week (i.e., new, waxing, full,
82 and waning moon) for eight weeks, and observed beach-spawning behavior at the spring
83 tide (Figures 1B,C; Video S1). After bringing live puffers back to the laboratory, we
84 collected the brain region containing the hypothalamus and pituitary (Figure 1D) at
85 around 19:00 (Japan Standard Time) and measured the gonadosomatic index [(GSI);
86 (gonad weight/body weight) × 100) (Figure 1E). Grass puffers are seasonal breeders, and
87 males develop gonads in early May [9]. Thereafter, they spawn every two weeks during the
88 spring tide, resulting in a significant decrease in the gonadal weight in the latter half of
89 the breeding season (Figure 1E). Despite the significant decrease in gonadal weight,
90 beach-spawning was observed until the full moon in mid-July when they exhausted their
91 available spermatids (Figures 1C,E; Figure S1).
92
93 **Identification of semilunar genes**
94 For each time point, total RNA was prepared from each brain sample and two
95 RNA samples were pooled as one biological replicate (6 fish in total, n = 3), and RNA-
96 seq analysis was performed using the DNBseq platform, generating an average of 5.41
97 Gb per sample. Genome sequences for the closely related tiger puffer (*Takifugu rubripes*)
98 are considered to be highly similar to those from the grass puffer [11]. Indeed, grass puffers
99 can hybridize with tiger puffers, and the reciprocal hybrids are viable and fertile [12].
100 Therefore, we used the tiger puffer genome (assembly fTakRub1.2) as a reference.

To validate our RNA-seq analysis, we first extracted the differentially expressed genes (DEGs) between individuals with high GSI (from the first four time points, n = 12) and low GSI (the latter four time points, n = 12) using the DEseq2 algorithms. This analysis identified 11 DEGs, including follicle-stimulating hormone β subunit (*fshb*) (Figures 2A,B; Figure S2A; Table S1). It has been reported that follicle-stimulating hormone (FSH) is important for gonadal development, whereas luteinizing hormone (LH) is pivotal for final maturation of the gonad and induction of spawning behavior in several fish species [13, 14]. The significant decrease in *fshb* expression (Figure 2B) followed by gonadal regression (Figure 1E) was consistent with the results of these previous studies .

We next extracted DEGs between individuals from the spring (new and full moon, n = 12) and neap tides (waxing and waning moon, n = 12). A total of 125 genes were identified as DEGs (Figure 2C). These 125 DEGs were grouped into two clusters (87 up- and 38 down-regulated genes at spring tide) based on their time-series expression profiles over the span of two consecutive lunar cycles (Figure 2D).

Kyoto Encyclopedia of Genes and Genomes (KEGG) pathway enrichment analysis of the 125 semilunar DEGs identified 'endocrine system', 'signal transduction', and 'signaling molecules and interaction', as the top three enriched pathways (Figure 2E). Specifically, we observed a significant overrepresentation of DEGs involved in 'neuroactive ligand–receptor interaction' and 'GnRH signaling' (Figure 2F) and up-regulation of hormone-related genes such as *gnrh1*, *lhb*, *cga*, growth hormone 1 (*gh1*), thyroid–stimulating hormone β subunit a (*tshba*), and progesterone receptor (*pgr*) in puffers collected at the spring tide (Figure 2G, Figure S2A, Table S2). The hypothalamus–pituitary–gonadal (HPG) axis is primarily responsible for regulating reproduction in various vertebrates, and *gnrh1*, *lhb*, and *cga* play pivotal roles in final maturation of the

gonads and induction of spawning behaviors in fish [13, 14].

In addition to these hormones and receptors, we found up-regulation of receptors for PGE (e.g., *ptger2a* and *ptger4a*) in puffers collected at the spring tide (Figure 2G, Figure S2B, and Table S2). $PGF_{2\alpha}$ is a 'hormonal pheromone' that induces LH secretion and spawning behavior in freshwater fish [15, 16, 17]. However, the presence of hormonal pheromones in marine species remains unclear [16]. We therefore hypothesized that PGE acts as a hormonal pheromone to induce beach-spawning behavior in grass puffers.

PGE_2 is secreted by puffers into the seawater during beach-spawning

Beach-spawning takes place repeatedly in groups of 10–60 fish consisting of one female and multiple males [8] (Video S1). At the height of spawning, seawater at the spawning site is stained white with the milt ejaculated by the males. To test whether PGE is secreted during beach-spawning, seawater was sampled at different distances from the center of the spawning site. Using liquid chromatography–tandem mass spectrometry, we detected PGE_2 at the center of the spawning site, but not 20 m from the center (Figures 3A-F). Although we also tried to detect PGE_2 metabolite, 15-keto-PGE_2 at the center of the spawning site, we failed (Figure S3). We then quantified the PGE_2 level at each sampling point using an ELISA. As expected, seawater from the center contained the highest levels of PGE_2 (6.28×10^{-11} M) (Figure 3G). The concentration of PGE_2 decreased as distance between the sampling point and center of the spawning site increased.

To further explore whether PGE_2 was derived from males or females, the level of PGE_2 was measured in squeezed milt and eggs. Although concentrations were higher in female-collected samples than male (4.6 fold), PGE_2 was found in both seminal and ovarian fluids (Table 1). PGE_2 was also detected in the eggs and spermatids, but the

concentrations were lower than in the ovarian and seminal fluids, respectively (Table 1). Thus, PGE_2 found in the seawater is secreted by both males and females during beach-spawning.

PGE_2 induces trembling behavior and activates olfactory sensory neurons

Grass puffers are wild animals, and handling them in the laboratory setting is extremely difficult. Captive propagation of wild grass puffers has not yet been achieved. Because the effects of pheromones are context dependent [16, 18], we attempted to mimic the natural beach in our laboratory. The proximate factor influencing the spawning site choice for grass puffers is the angle of inclination of the beach (6.68–11.30°) [19]. Therefore, we prepared an artificial beach with a 9° angle of inclination in an experimental tank equipped with a wave-making device. Our preliminary experiments demonstrated that the effect of PGE_2 on puffer behavior does not depend on the sex ratio of puffers within the tank. Therefore, we examined the effect of PGE_2 for each sex separately for simplicity (n = 11 or 12). Using a peristaltic pump, vehicle or PGE_2 was applied to the tank every 5 min. Unlike $PGF_{2\alpha}$ in freshwater fish, no attractive response was induced by PGE_2. However, both males and females began showing trembling behavior by PGE_2 at 10^{-11} M (final concentration within the tank) (Figure 4A, Video S2). The number of responding fish increased in a dose-dependent manner (Figure 4B, Video S3). Importantly, the dose of PGE_2 that induced trembling behavior was consistent with the concentrations detected in seawater.

The hormonal pheromone prostaglandin activates olfactory sensory neurons in freshwater fish [16, 17]. Therefore, we examined the PGE_2-mediated activation of olfactory sensory neurons using multiplex fluorescent *in situ* hybridization. In olfactory epithelium

of grass puffers, many islets containing ciliated and microvillous neurons are surrounded by non-ciliated cells (Figure 4C) [20]. The surrounding non-ciliated cells include the crypt neurons. When we administered PGE_2, we observed colocalization of the neuronal activation marker c-*fos* with *ptger2a* in non-ciliated cells, but little expression of c-*fos* in the vehicle control (Figures 4D,E). PGE_2-induced c-*fos* expression was not observed in the adjacent *ptger2a* negative cells (Figure 4E). Expression of *ptger4a* was not detected in olfactory epithelium. Specific signal for negative control probe was not detected (Figure S4A).

Spatial transcriptomics depicts the expression sites for the semilunar genes

To further explore the mechanism that regulates the lunar-synchronized transcription of semilunar genes, we searched for semilunar transcription factors. Among the 125 semilunar genes, we identified 12 transcription factors. To examine overlaps in the expression sites between these 12 semilunar transcription factors and semilunar hormone genes, we used spatial transcriptomics analysis using a Visium Spatial Gene Expression platform (10X Genomics). This technique, which uses spatially barcoded poly-T capture probes, enables RNA-seq from tissue sections while retaining anatomical information [21]. We obtained two sagittal cryo-sections from the brain of male grass puffer collected at spring tide (Figure 5A). A total of 3,095 spots were detected with 111,623 mean reads per spot and 11,947 median Unique Molecular Identifiers (UMIs) (Figure S5A,B). We used a Uniform Manifold Approximation and Projection (UMAP) plot to reduce the complexity of the spatial transcriptomics data and visualized the molecular relationship between the clusters in a 2D space (Figure 5B). This approach organized the puffer brain

197 regions into 13 transcriptionally distinct clusters, and comparisons between each cluster
198 allowed for the identification and visualization of genes unique to several clusters (Figure
199 S5C). We found that cluster 3 contains the anterior parvocellular nucleus of preoptic area
200 (POA) and ventral part of ventral telencephalic area (Vv), whereas cluster 9 contains the
201 periventricular region of diencephalon (Pr). Cluster 13 contained the pituitary (Pit) and
202 ventral zone of periventricular hypothalamus (Hv). When we visualized expression sites
203 for the semilunar hormone genes, we observed expression of *gnrh1* in the POA (cluster
204 3) and the Hv (cluster 13), as expected (Figure 5C). Strong expression of the semilunar
205 pituitary hormone genes *lhb*, *cga*, and *gh1* was observed in the pituitary (cluster 13). As
206 reported in previous studies [22, 23, 24], expression of these pituitary hormone genes was not
207 limited to the pituitary, and weak expression was also confirmed in other part of the brain
208 such as POA, Vv (cluster 3) and Pr (cluster 9).
209 Expression levels were very low for eight of twelve semilunar transcription
210 factors (Figure S6). By contrast, expression levels were high for the remaining four
211 semilunar transcription factors (*cebpd*, *crema*, *mafk*, and *rnf227l*) (Figure 5C). Among
212 these, expression of *cebpd* (CCAAT enhancer binding protein delta) and *crema* (cAMP
213 responsive element modulator a) was observed in POA, Pr, Pit, and Hv (clusters 3, 9, and
214 13). On the other hand, *mafk* (MAF bZIP transcription factor K) was observed in Pr, Pit,
215 and Hv (clusters 9 and 13), while *rfn227l* (RING finger protein 227-like) was observed
216 in Pr (cluster 9) (Figure 5C).
217
218 **The semilunar transcription factor cebpd regulates *gnrh1* transcription**
219 We next aimed to identify the potential transcription factor that regulates semilunar *gnrh1*
220 expression. The gnrh1 neuronal population present in the POA projects to the pituitary

and regulates gonadotropin secretion [25]. As aforementioned, only *cebpd* and *crema* were expressed in the POA (Figure 5C, cluster 3). The neighboring gene encoding potassium channel tetramerization domain containing 9 (*kctd9*) is located 541 bp upstream of *gnrh1*. To statistically identify the potential binding sites for cebpd and crema (Figure 6A), we applied the Sequence Motif Location Tool (MoLoTool) to the upstream sequences of the grass puffer *gnrh1* using the default recommended p-value < 0.0001. Although we found one binding motif for cebpd, no binding motif for crema was identified. To examine the functional significance of cebpd and crema, we prepared a luciferase reporter construct containing the upstream region of grass puffer *gnrh1* (*gnrh1* WT). We analyzed the promoter activity using Chinese hamster ovary (CHO) cells. As expected, co-transfection of *cebpd*, but not *crema*, induced *gnrh1* reporter activity (Figure 6B). When compared with the binding motif for crema, the consensus binding motif for cebpd is fuzzy (Figure 6A). Because motif finding software's sensitivity to find fuzzy DNA motifs is low, we employed the degenerate sequences for cebpd in our analysis to avoid missing potential critical binding sites. As a result, multiple potential binding sites for cebpd were identified in the upstream region of the *gnrh1* gene (Figure 6C). The deletion study suggested that a potential binding motif located at around -100 bp plays a critical role (Figure 6C). This result was further validated by mutating this binding motif (Figure S7). To further examine the co-expression of *cebpd* and *gnrh1*, we examined detailed distribution using multiplex fluorescent *in situ* hybridization. No specific signal was observed in the negative control (Figure S4A), and co-expression of *cebpd* and *gnrh1* was observed within the POA (Figure 6D, Figures S4B,C). These results suggested that grass puffer *gnrh1* is induced by cebpd.

Discussion

Many organisms living along coastlines synchronize their reproduction with lunar cycles. The dramatic sight of beach spawning at the water's edge has attracted great interest for a long time. However, how animals can synchronize their reproduction to astronomical lunar cycles and accomplish the spectacular beach-spawning event remained a mystery. Our time-series RNA-seq analysis of the hypothalamus and pituitary of the grass puffer identified 125 semilunar genes (Figure 2). Among them, genes involved in the HPG axis that are essential for spawning behavior were activated every two weeks during the spring tide. This result was somewhat unexpected; since grass puffers are seasonal breeders, we predicted that their HPG axis would be continuously activated during their breeding season from mid-May to mid-July. However, the present results clearly demonstrated that the HPG axis of the male grass puffer is activated every two weeks during the spring tide.

In addition to the genes for reproductive hormone, we found semilunar rhythmicity in the transcription of PGE receptors. Although hormonal pheromones are well understood in freshwater fish such as the goldfish, carp, and zebrafish [15, 16, 17], the identity of hormonal pheromone remains unclear in marine species [16]. In goldfish, eggs in the oviduct induce the synthesis of $PGF_{2\alpha}$ at ovulation, which acts on the brain to stimulate female sex behavior. During oviposition, $PGF_{2\alpha}$ is released into the water to function as a postovulatory hormonal pheromone that stimulates males for courtship, spawning behavior, and further LH release. On the basis of these findings in freshwater fish, we predicted that prostaglandin would also act as hormonal pheromone in the grass puffer to induce beach-spawning. Indeed, we found PGE_2 in the seminal and ovarian fluids and the seawater collected at the center of the spawning site (Figure 3, Table 1). Furthermore, PGE_2 administration activated olfactory sensory neurons expressing EP2

prostaglandin receptor (*ptger2a*) and induced vigorous trembling behavior as 'releaser pheromones' that evoked rapid behavioral responses in the artificial tank (Figure 4). However, puffers did not spawn eggs or milt in the tank. The effects of pheromones are context-dependent and are influenced by many ecological factors [16, 18]. Although we tried to mimic the natural spawning site as closely as possible (e.g., slope of the beach, waves, pebbles, photoperiod, water temperature, and time of day of the behavior experiment), it was still an artificial environment within the laboratory. In addition, most fish pheromones are mixtures [16, 18]. Therefore, it is possible that 'primer pheromones', which evoke critical endocrinological responses such as gonadal steroid hormones, were insufficient to induce full beach-spawning behavior in our artificial environment. Nevertheless, these results clearly suggest that the hormonal pheromone PGE_2, which is released into seawater by spawning males and females, triggers the synchronized beach-spawning behaviors observed in the surrounding individuals.

The mechanism that drives lunar-regulated rhythmicity remains a mystery in any organisms to date. Our spatial transcriptomics and multiplex flurorescent *in situ* hybridization analysis showed co-localization of the semilunar transcription factor *cebpd* and *gnrh1* (Figures 5, 6). Furthermore, cebpd induced the promoter activity of *gnrh1*, suggesting that cebpd regulates semilunar rhythmicity in the grass puffer. The synchronization of reproduction to the lunar cycle is not limited to organisms living along the shoreline. For example, wildebeest mating [26] and calf delivery in cows [27] are synchronized with the lunar cycle. It is particularly noteworthy that menstrual cycles, sleep–wake cycles, and manic–depressive cycles are synchronized with the moon cycle in humans, and human biology and behavior are generally affected by the lunar cycle [28, 29, 30]. Human CEBPD (C/EBPδ) modulates many biological processes, including cell

differentiation, proliferation, growth arrest, and cell death, and its role in inflammation and cancer has recently been highlighted [31]. Because *cebpd* is highly conserved in the animal kingdom, its role in the regulation of lunar rhythms in other animals is worth investigating in future studies.

Acknowledgements

We thank Drs. Daisuke Kurokawa, Taeko Nishiwaki-Ohkawa, Naohiro Kon, and Hanako Hagio for helpful discussion. This work was supported in part by the Aschoff and Honma Memorial Foundation, Kihara Memorial Yokohama Foundation, Toyota Boshoku Corporation, and Nagoya University Research Fund to T.Yo., and "Grant-in-Aid for Scientific Research (B)" (20H03288) to H.A. and T.Yo. WPI-ITbM is supported by the World Premier International Research Center Initiative (WPI), MEXT, Japan.

Author contributions

T.Yo. conceived the study. T.Yo., J.C., Y.K. and Y.J.G. designed the research. J.C., Y.K., K.O., T.Ya., Y.J.G., T.N., M.M., Y.F., Y.N., N.Y., A.Sa., and T.Yo. conducted the experiments and analyzed the data. Y.S., H.A., A.Su. and K.T. provided new material and methods. J.C., Y.K., K.O., T.Ya., A.Sa. and T.Yo. wrote the manuscript. All authors discussed the results and commented on the manuscript. T.Yo. supervised the study.

Declaration of interests

The authors declare no competing interests.

Inclusion and diversity

We worked to ensure diversity in experimental samples through the selection of the genomic datasets. While citing references scientifically relevant for this work, we also actively worked to promote gender balance in our reference list.

Figure legends

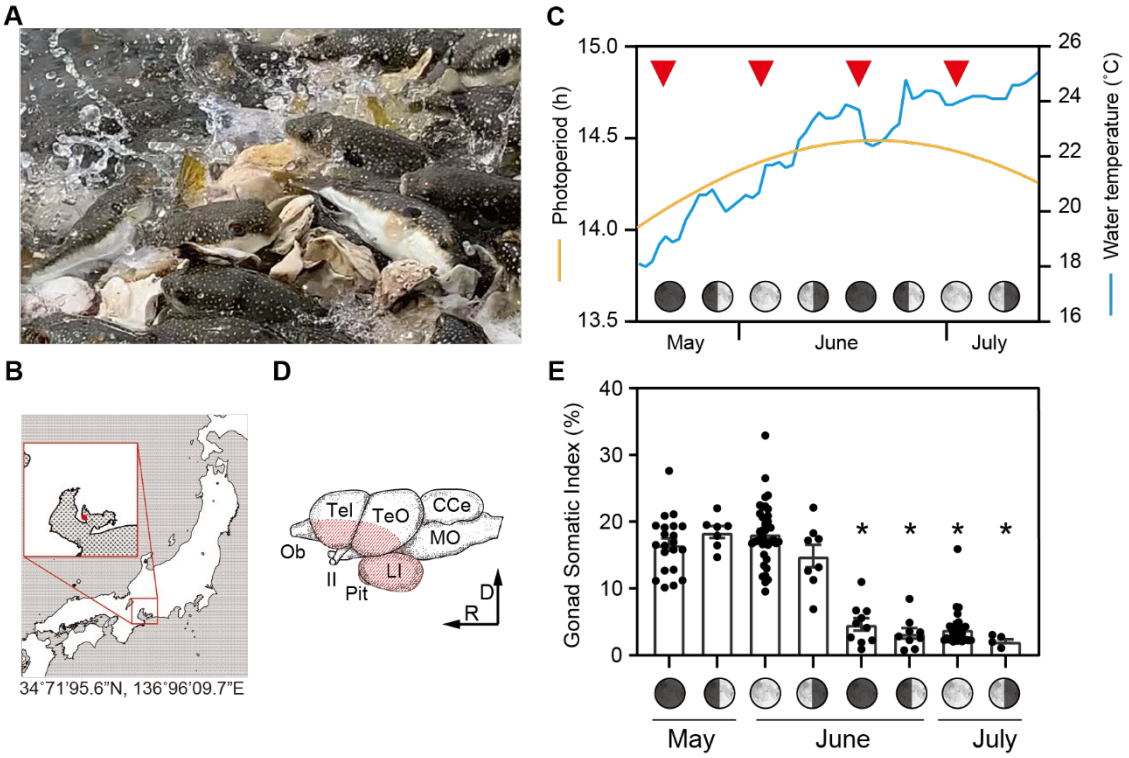

Figure 1. Male grass puffers are semilunar spawners.

(A) Beach-spawning of grass puffers at the water's edge.

(B) Map showing the spawning site (red dot) for sample collection.

(C) Samples were collected every week (i.e., new, waxing, full, and waning moons) for two months from the middle of May to the middle of July in 2020. The changes in daylength and seawater temperature during the breeding season are shown. Spawning was observed during the spring tide (arrowheads).

(D) Schematic diagram of the brain region (hatched red area) dissected for RNA-seq analysis. D: dorsal; R: rostral; CCe: corpus cerebelli; LI: lobus inferior; MO: medulla oblongata; Ob: olfactory bulb; Pit: pituitary; Tel: telencephalon; TeO: optic tectum; II: optic nerve.

(E) Changes in GSI during the breeding season (Brown-Forsythe test, $F_{(7, 57.56)} = 82.38$, $p < 0.0001$, Dunnett's T3 test, $^{*}p < 0.0001$ vs. week 1, n = 7–39).

See also Figure S1, Video S1.

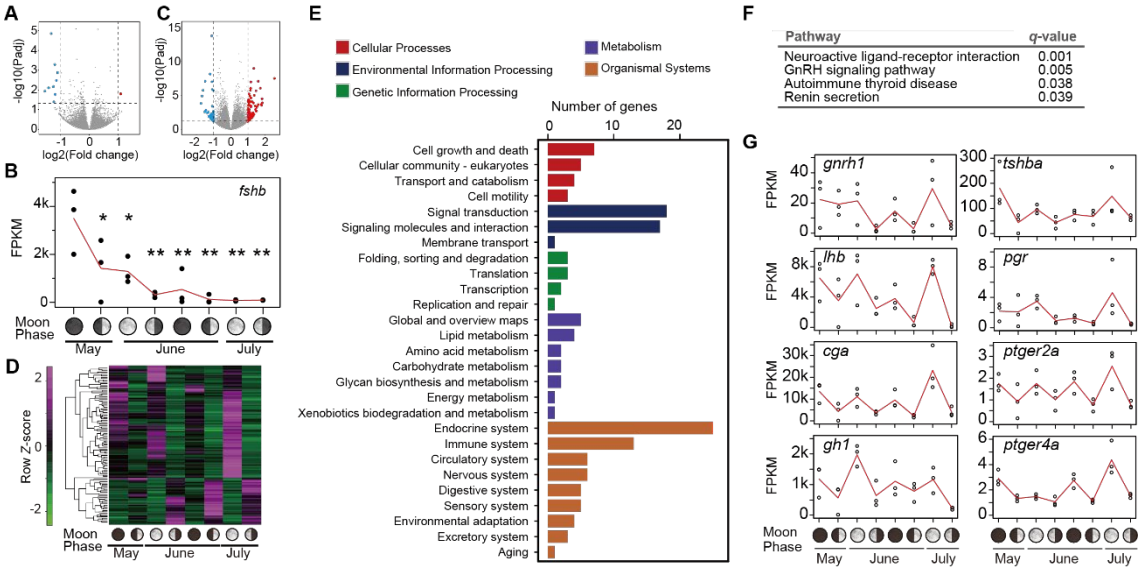

338

339 **Figure 2. Identification of semilunar genes.**

340 (A) Identification of 11 DEGs between individuals with high (weeks 1–4) and low
341 (weeks 5–8) GSIs.

342 (B) Reduction in *fshb* expression levels over the course of the breeding season.
343 Red lines indicate the means, and individual values are shown using black dots
344 (one-way ANOVA, $F_{(7, 16)} = 7.379$, $p < 0.001$, Dunnett's test, $^{*}p < 0.05$, $^{**}p < 0.01$
345 vs. week 1, n = 3).

346 (C) Identification of 125 DEGs between the spring (weeks 1, 3, 5, and 7) and
347 neap (weeks 2, 4, 6, and 8) tides.

348 (D) Heatmap showing the temporal expression profile for 125 semilunar genes.

349 (E) KEGG pathway classification results of 125 semilunar genes.

350 (F) KEGG pathway functional enrichment results of 125 semilunar genes.

351 (G) Temporal expression profiles for semilunar hormone and PGE_2 receptor
352 genes (n = 3).

353 See also Figure S2, Tables S1 and S2.

354

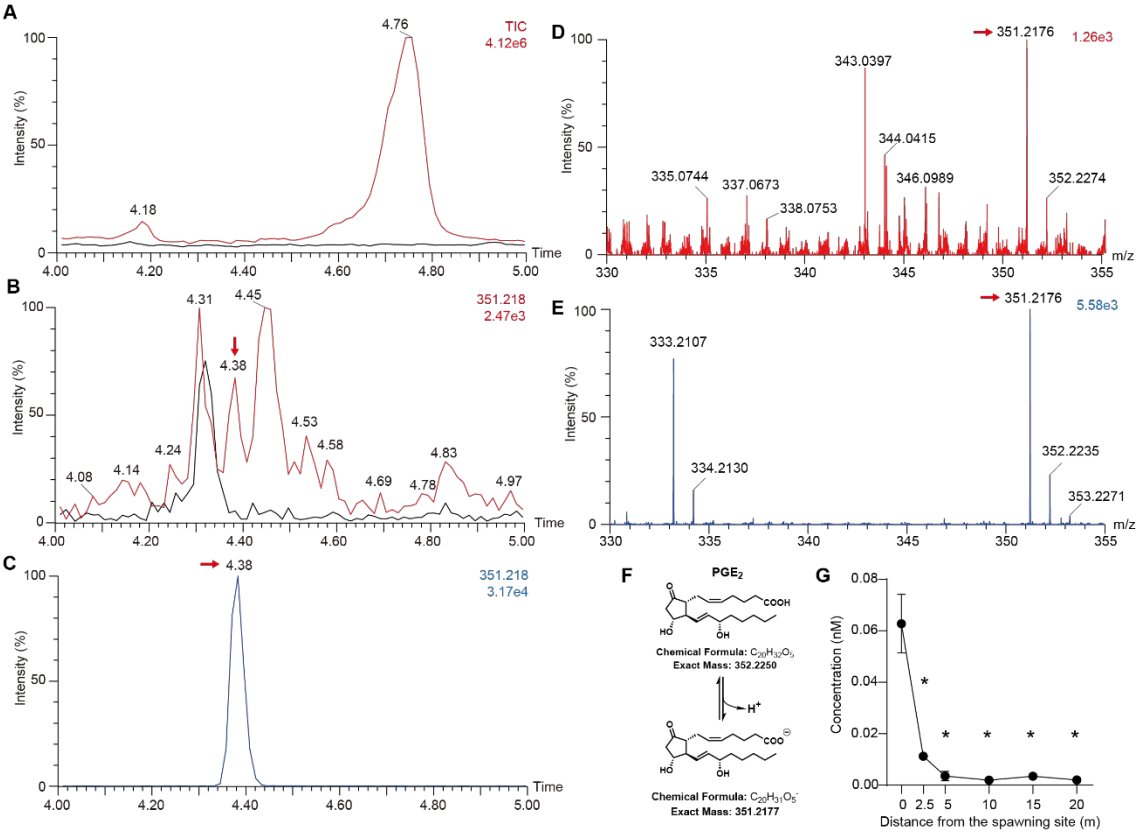

Figure 3. PGE_2 is secreted by puffers into the seawater during beach-spawning

(A) Total ion chromatogram (TIC) of the seawater at 0 m (red line) and 20 m (black line).

(B) Mass chromatogram filtered using *m/z* 351.2177 (± 0.5 ppm) for seawater at 0 m (red line) and 20 m (black line).

(C) Mass chromatogram for the authentic PGE_2 (10 nM in 50% aqueous MeOH).

(D) Mass spectrum of seawater at the spawning site. The observed mass (*m/z* 351.2176 $[M-H]^-$) was obtained at the same retention time (Rt = 4.37 min) as the authentic PGE_2 and was consistent with the authentic one (*m/z* 351.2176 $[M-H]^-$, accuracy: 0.2847 ppm)

(E) Mass spectrum for the authentic PGE_2.

(F) Exact masses of the neutral and ionized form of PGE_2.

(G) PGE_2 concentrations at different sampling points were measured using ELISA (one-way ANOVA, $F_{(5, 12)} = 25.99$, $p < 0.0001$, Dunnett's test, $^*p < 0.0001$ vs. 0 m, n = 3).

See also Figure S3, Table 1, and Video S1.

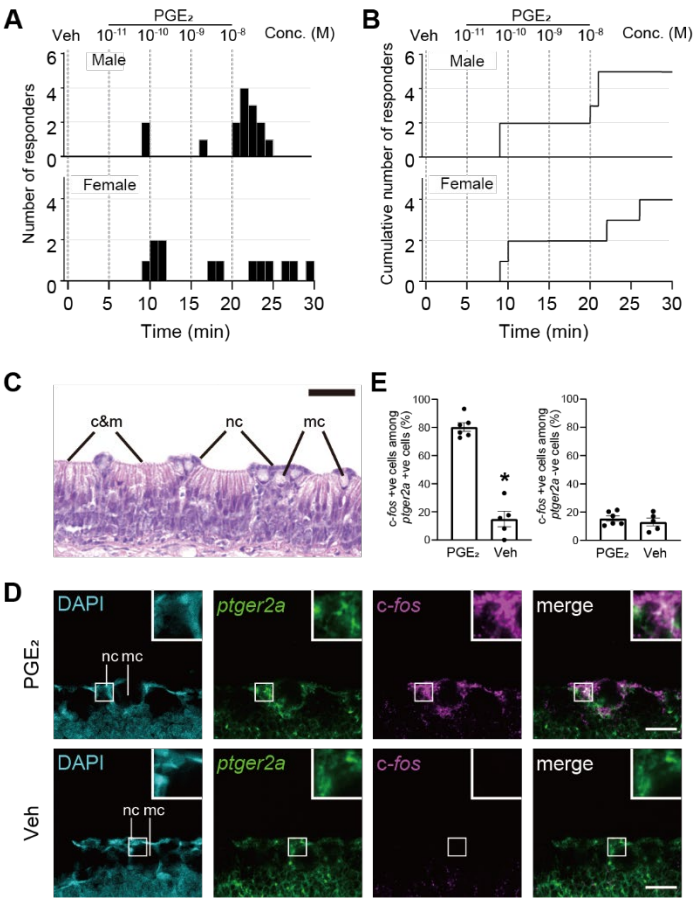

Figure 4. PGE_2 induces trembling behavior and activates olfactory sensory neurons

(A) Quantification of the fish showing the trembling behavior (top: male, n = 12; bottom: female, n = 11).

(B) Cumulative records for fish showing the trembling behavior (top: male, n = 12; bottom: female, n = 11).

(C) Olfactory epithelium of grass puffer stained with HE. Islets consisting of ciliated and microvillous neurons (c&m) are surrounded by non-ciliated neurons (nc) including crypt neurons. mc: mucous cells. Scale bar: 20 μm.

(D) PGE_2 activates non-ciliated neurons (nc) expressing *ptger2a*. Multiplex fluorescent *in situ* hybridization for c-*fos* and *ptger2a* from the olfactory epithelium of PGE_2- and vehicle (Veh)-treated fish (final concentration: 10^{-9} M). mc: mucous cells. Scale bar: 20 μm.

(E) Percentages of c-*fos* positive (+ve) cells among *ptger2a* +ve cells (left) or adjacent *ptger2a* negative (-ve) cells (right) from the olfactory epithelium of PGE_2- and vehicle (Veh)-treated fish (final concentration: 10^{-9} M). Values represent mean ± SEM. (*ptger2a* +ve cells: Welch's *t*-test, $t_{(6.346)} = 10.32$, $^*p <$

0.0001; *ptger2a* -ve cells: Welch's *t*-test, $t_{(7.543)} = 0.7572$, $p = 0.4719$; n = 6 in PGE_2- treated group and n=5 in vehicle-treated group).
See also Figure S4 and Videos S2, S3.

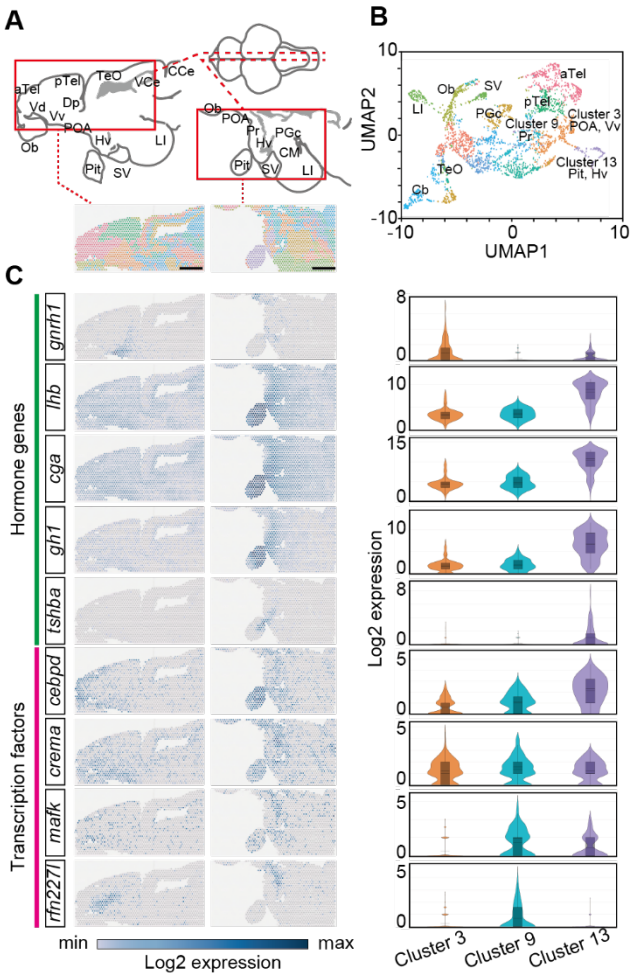

Figure 5. Spatial transcriptomics depicts the expression sites for the semilunar genes.

(A) Schematics of the puffer brain depicting the brain sections (red rectangles) used for spatial transcriptomics (top) and visual depiction of the 13 clusters (bottom). Scale bar: 1 mm.

(B) UMAP showing 13 clusters across 3,095 dots. Each dot corresponds to a unique barcoded plot.

(C) Left and right panels show the spatial expression and violin plot for semilunar hormones and transcription factors, respectively.

See also Figures S2, S5, and S6.

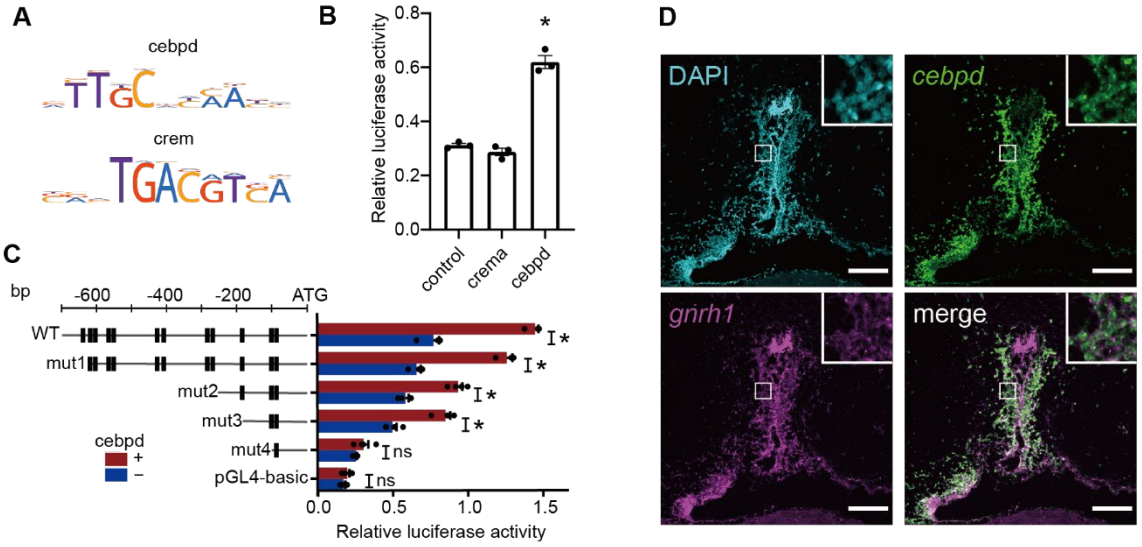

Figure 6. The semilunar transcription factor cebpd regulates *gnrh1* transcription

(A) DNA motif sequence logo for cebpd and crem from HOCOMOCO database.

(B) Promoter activity for grass puffer *gnrh1*. Wild type (WT) reporter fused to the luciferase gene were assayed for the activities with *cebpd* or *crema* co-transfection. Each value represents the mean + SEM for a single assay (one-way ANOVA, $F_{(2, 8)} = 126.4$, $p < 0.0001$, Dunnett's test, $^{*}p < 0.0001$ vs. control, n = 3).

(C) Promoter activity for grass puffer *gnrh1*. Wild type (WT) and deletion mutant reporters fused to the luciferase gene were assayed for their activities with or without *cebpd* co-transfection. The location of potential cebpd binding sites is indicated by black boxes. Each value represents the mean + SEM for a single assay (Welch's *t*-test, $t_{(4.981)} = 15.27$ [WT], $t_{(3.718)} = 12.80$ [mut1], $t_{(5.597)} = 9.725$ [mut2], $t_{(5.783)} = 8.282$ [mut3], $t_{(3.316)} = 1.668$ [mut4], $t_{(4.997)} = 1.216$ [pGL4-basic], $^{*}p < 0.001$, n = 3–4).

(D) Representative confocal images of POA showing co-expression of *cebpd* and *gnrh1*. Scale bar: 100 μm.

See also Figures S4, S7 and Table S3.

Table 1. Concentrations of PGE_2 measured by ELISA

Samples	**PGE_2 (mean ± SEM, n = 3)**
Ovarian fluid	24.11 ± 6.67 nM
Eggs	11.5 ± 2.68 pg/mg sample
Seminal fluid	5.2 ± 1.24 nM
Spermatids	0.66 ± 0.14 pg/mg sample

STAR METHODS

Resource availability

Lead contact

Further information and requests for resources and reagents should be directed to the lead contact Takashi Yoshimura (takashiy@agr.nagoya-u.ac.jp).

Materials availability

This study did not generate new unique reagents.

Data and code availability

・The RNA-seq data sets generated in this study have been deposited in the NCBI's Gene Expression Omnibus and are available through GEO series accession numbers GSE186499 and GSE186818. Data reported in this study will be shared by the lead contact upon request.

・This paper does not report original code.

・Any additional information required to reanalyze the data reported in this paper is available from the lead contact upon request.

Experimental model and subject details

Animals

Male adult grass puffers were obtained from Minamichita, Japan (Figure 1B) during the spring and neap tides every week for eight weeks from the middle of May to the middle of July in 2020 (Figure 1C). All animal studies were carried out in accordance with ARRIVE guidelines and all methods were in compliant with relevant guidelines and

regulations and were approved by the Animal Experiment Committee of Nagoya University.

Method details

RNA extraction and sequencing

Total RNA was prepared from the brain area containing the hypothalamus and pituitary (Figure 1D) using the RNeasy Lipid Tissue Mini Kit (Qiagen). Equal amounts of the extracted RNA from two individuals were pooled as one biological replicate, and three replicates were used for the RNA-seq analysis for each sampling timepoint. For construction of the library, mRNA was first purified from the total RNA using poly-T oligo-attached magnetic beads and was then fragmented, after which cDNA synthesis was performed. The synthesized cDNA was used for the preparation of PE100 strand-specific sequencing libraries, which were subsequently sequenced using a DNBseq platform to generate 50–60 million reads for each library (BGI). Clean reads were mapped using Bowtie2 and the average mapping ratio was 80.75%. The gene expression level for each sample was calculated with RSEM. We used DEseq2 algorithms to detect differentially expressed genes (DEGs).

Quantification of gene expression

The raw reads were first filtered to remove reads with adaptors, reads with unknown bases [(N)>0.1%], and low-quality reads which contain >40% of the bases with a Phred score <20 using the BGI internal program SOAPnuke [32]; the remaining reads were defined as the ‘clean reads’ and were used for further analysis. Next, the clean reads were mapped to the reference genome fTakRub1.2 using HISAT2 [33]. The transcripts were assembled

using StringTie [34] and compared to the reference annotation using Cuffcompare [35], and the novel transcripts were identified. The coding potentials for these novel transcripts were predicted using CPC [36], and the predicted coding transcripts were subsequently merged with the reference annotation to generate the complete reference for downstream mapping. The clean reads were then mapped to this new reference using Bowtie2 [37], and gene expression was quantified using the RSEM program [38] and presented as the Fragments Per Kilobase of transcript per Million mapped reads (FPKM).

Identification of DEGs

In order to identify the DEGs associated with differences in the size of the gonads, we grouped the samples collected at weeks 1–4 as one group and the samples from weeks 5–8 as another group. In addition, samples from weeks 1, 3, 5, and 7 were grouped as the spring tide group, and samples from weeks 2, 4, 6, and 8 were grouped as the neap tide group to identify the DEGs with semilunar rhythmicity. DEseq2 [39] was used to detect the DEGs for each contrast using an adjusted *p*-value (Padj) of ≤0.05 and log2 fold change of ≥1.

GO and KEGG enrichment analysis

Reference sequence was aligned against the NCBI non-redundant (NR) protein database using the blastx function in the DIAMOND program [40], and the associated gene ontology (GO) annotations for the best homologues were extracted. The same DIAMOND blastx function was performed to search for the annotated proteins in the Kyoto Encyclopedia of Genes and Genomes (KEGG) database. Next, the identified DEGs were classified based on these GO and KEGG annotations, after which enrichment analysis was

501 performed using the phyper function in R, and the FDR was calculated for each *p*-value.
502 We defined pathways with an FDR<0.01 as significantly enriched.
503
504 **Quantitative real-time PCR (qPCR)**
505 Total RNA used for the RNA-seq analysis was reverse transcribed into cDNA using the
506 High-Capacity cDNA Reverse Transcription Kit (ThermoFisher Scientific). qPCR was
507 performed using a real-time qPCR system (Quant Studio 3, Applied Biosystems) with a
508 10 μl reaction containing SYBR Green PCR Master Mix (ThermoFisher Scientific), 0.3
509 μM primers, and cDNA template. The cycling program was as follows: initial
510 denaturation for 10 minutes at 95°C followed by 40 cycles of 95°C for 15 seconds and
511 60°C for 1 minute. *gapdh* was used as the housekeeping gene, and the average expression
512 level for each gene at week 1 was assumed to be 1 for the comparison between relative
513 expression levels. The primers used in this study are listed in Table S3.
514
515 **Histology of the testes**
516 Testes from grass puffers were cut into small pieces and fixed using 4% paraformaldehyde
517 in phosphate-buffered saline (pH 7.4). Paraffin-embedded sections were cut at a thickness
518 of 5 μm and stained with hematoxylin–eosin (HE) for microscopic observation (BZ-X800,
519 Keyence).
520
521 **Prostaglandin measurement**
522 Seawater was sampled at different distances (0, 2.5, 5, 10, 15, and 20 m) from the center
523 of the spawning site (0 m) and was transported to the lab on dry ice. Squeezed eggs and
524 milt were obtained from mature wild grass puffers. All samples were collected during the

spring tide and were kept at –80°C before sample preparation. Squeezed eggs were filtered through a 100 μm pluriStrainer Mini filter (pluriSelect) to separate the ovarian fluid from the eggs, and squeezed milt was centrifuged at 10,000 rpm for 5 minutes at 4°C to separate the spermatids and seminal fluid.

Liquid chromatography–tandem mass spectrometry (LC-MS/MS)

PGE_2 was purchased from Cayman Chemicals. LC-MS–grade methanol (MeOH), acetonitrile, distilled water, and acetic acid were obtained from KANTO KAGAKU. Seawater was sampled at the spawning site and transported to the laboratory on dry ice. First, 10 ml of seawater was lyophilized. Next, prostaglandin was extracted from the samples using 1 ml of MeOH. The methanol extracts were diluted with the same amount of distilled water and filtered with a modified polyethersulfone ultrafiltration membrane (nanosep blue 10K, PALL) to remove insoluble material (inorganic salts and proteins). The filtrates were five-fold concentrated over seawater and directly used for LC-MS/MS analysis. All procedures were performed on ice. LC-MS/MS analysis was performed using ultra performance liquid chromatography (ACQUITY UPLC H-Class, Waters) and a quadrupole time-of-flight mass spectrometer (G2-XS QTof Xevo, Waters). Chromatographic separation was achieved after extensive optimization of the mobile phase composition, gradient conditions, and run time. All the samples were separated using an ACQUITY UPLC CSH C18 Column (1.7 μm, 2.1 mm × 100 mm, Waters), and a mobile phase A (0.1% acetic acid in distilled water) and mobile phase B (acetonitrile), and a flow rate of 0.3 ml/minute. All samples were separated using the following solvent composition. The initial mobile phase composition was 30% B. The concentration was gradually increased to 100% B over 7 minutes, held at 100% B for 3 minutes, and returned

549 to the initial condition (30% B) over 0.1 minutes, followed by 4.9 minutes of equilibration
550 prior to the next analysis. The injection volume for all samples was 5 µl. Mass
551 spectrometry was performed under electrospray ionization (negative mode) with the
552 following source ionization parameters: capillary voltage, 2.0 V; source gas, 150°C with
553 a 50 L/h flow rate; and desolvation gas (nitrogen), 550°C with a 900 L/h flow rate. PGE_2
554 was identified in the seawater samples, and its retention time and fragmentation pattern
555 were compared to those obtained for the PGE_2 standard sample.
556
557 **Enzyme-linked immunosorbent assay (ELISA)**
558 Solid Phase Extraction (SPE) is a method for purifying non-polar analytes, including
559 prostaglandins, from other impurities, such as cells and water-soluble molecules, in
560 solution. Therefore, eight-fold concentrated prostaglandins were prepared from 5 ml of
561 seawater using 500 mg SPE Cartridges (C-18) (Cayman Chemical), and were
562 resuspended in 625 µl ELISA buffer. One hundred milligrams of filtered eggs and
563 spermatids were homogenized in 1 ml 0.1 M phosphate buffer (pH = 7.4, FUJIFILM)
564 containing 1 mM EDTA (Nippon Gene) and 10 µM indomethacin (Tocris) using a Multi-
565 beads Shocker (Yasui Kikai). The homogenate was centrifuged at 10,000 g for 2 minutes
566 at 4°C, and the supernatant was subsequently collected. Ovarian and seminal fluid
567 samples were applied to the downstream ELISA assays directly. Three biological
568 replicates were included for each assay and all the samples were diluted with ELISA
569 buffer so that the concentrations were within the measurable range. The Prostaglandin E_2
570 ELISA kit – Monoclonal (Cayman Chemical) was used to quantify the PGE_2 levels in the
571 prepared samples, and the final absorbance was measured using a SpectraMax i3 Multi-
572 Mode Detection Platform (Molecular Devices). Prostaglandin concentrations are

presented in nanomolar (nM) for seawater and ovarian and seminal fluids, and in picogram/milligram sample weight (pg/mg) for eggs and spermatids.

Behavioral assay

Fish were kept under long day conditions (14 hours light and 10 hours dark), and the water temperature was ~22°C to mimic their breeding season conditions. Because they spawn at around 14:00, male or female grass puffers (n = 12 or 11, respectively) under breeding conditions were introduced to an experimental tank (120 cm W × 60 cm D × 60 cm H) filled with 70 L of artificial seawater with a salinity of 28–30 ppt at around 13:30 for habituation. A slope mimicking a natural beach with 9° incline was made using pebbles [19]. To mimic waves at the spawning beach, waves were produced using a wave-making device (Fantastic wave ZX8000, MMC Planning). After 30-minute habituation, 1 ml vehicle (14% ethanol dissolved in seawater; the final ethanol concentration in the tank was 0.0002%) was applied as a negative control using a peristaltic pump (MP-2100, EYELA). Five minutes after vehicle administration, PGE_2 (stock solutions dissolved in ethanol) was prepared fresh with seawater before the experiment and was applied to the tank every 5 minutes. The final concentration of PGE_2 in the tank was increased incrementally as follows: 10^{-11} M, 10^{-10} M, 10^{-9} M, 10^{-8} M. Immediately after each administration, 1 ml of seawater was pushed through the pump tubing to ensure that the full volume of PGE_2 was dispensed into the tank. Puffer behavior was recorded using a video camera (HC-V480MS, Panasonic). Individual fish were distinguished using a small colored ribbon tag. Because trembling behavior typically lasts for 10 seconds during beach-spawning (Video S1), vigorous trembling that lasts for more than 10 seconds was defined as the trembling behavior. Trembling behavior was counted at 1-minute time

resolution in each behavioral assay.

Effects of PGE_2 on c-*fos* induction

Male or female grass puffers under breeding condition (n = 3) were introduced into a tank (30 cm W × 18 cm D × 24 cm H) filled with 10 L of artificial seawater. They were acclimated in the tank for 30 minutes. After acclimation, 1 ml of vehicle or 1 ml of 10^{-5} M PGE_2 (Cayman Chemicals) was applied using a peristaltic pump (MP-2100, EYELA) so that the final concentration in the tank was 10^{-9} M. Immediately after administration, 1 ml of seawater was pushed through the pump tubing to ensure that the full volume of PGE_2 was dispensed into the tank. Fifteen minutes after administration, the fish were euthanized using 0.05% 3-aminobenzoic acid ethylester methanesulfonate salt (MS222), and the olfactory epithelium was dissected out and fixed using 4% paraformaldehyde in phosphate-buffered saline (pH 7.4).

Multiplex fluorescent *in situ* hybridization

Paraffin-embedded sections were cut at a thickness of 5 μm for multiplex fluorescent *in situ* hybridization using the RNAscope Multiplex Fluorescent Reagent kit v2 (Advanced Cell Diagnostics). Probes for c-*fos, ptger2a, ptger4a, cebpd,* and *gnrh1* were prepared based on the sequences for XM_029849358.1, XM_011606140.2, XM_029830130.1, XM_003975262.3, and XM_029829752.1, respectively. The bacterial gene *DapB* (accession number EF191515) was used as negative control to assess background signals. For the olfactory epithelium, Opal520, Opal620, and Opal690 were used to visualize the signals for *ptger4a, c-fos*, and *ptger2a*, respectively. For the POA, Opal570 and Opal620 were used to visualize the signal for *gnrh1* and *cebpd*, respectively. For negative control

slides, Opal570 was used to visualize the signal for *DapB*. Slides were processed as described in the RNAscope protocol. A confocal laser scanning microscopy system (TCS-SP8, Leica) equipped with a pulsed white light laser (WLL, 80 MHz) and a HC PL APO CS2 20×/0.75 objective lens was used for fluorescence imaging of the olfactory epithelium (Figure 4D) and POA (Figure 6B). The fluorescence signals for DAPI, Opal520, Opal570, Opal620, and Opal690 were collected at 420–460 nm, 480–530 nm, 530–570 nm, 600–650 nm, and 680–740 nm using excitation at 405 nm, 470 nm, 514 nm, 594 nm, and 670 nm, respectively. Images were processed using Fiji image processing software [41].

Spatial transcriptomics

Fresh brains from male grass puffers were frozen in the optimal cutting temperature (OCT) compound (FSC 22 clear, Leica) using dry ice. Spatial transcriptomic slides had 5,000 spots (diameter: 55 μm; center-to-center distance: 100 μm) per 6.5×6.5 mm square (Visium spatial gene expression slide, 10X Genomics). Two sagittal sections with 10 μm thickness were cut onto one square of a spatial transcriptomic slide using a cryostat (CM3050 S, Leica) and were stored at –80°C for one day. Staining, permeabilization, reverse transcription, cDNA amplification, and library construction were performed following the Visium user guide (Rev. C) and using the Visium spatial gene expression reagent kits (10X Genomics). After HE staining, HE images were immediately captured (BZ-X800, Keyence). Time for permeabilization was 12 minutes using a thermal cycler (T100, Bio-Rad). The number of cycles for cDNA amplification was 14 with a real-time qPCR system (Quant Studio 3, Applied Biosystems). The constructed library was treated using the NovaSeq 6000 S4 reagent kit and the NovaSeq Xp 4-Lane kit (Illumina) and

was sequenced using the NovaSeq 6000 platform (Illumina) using paired-end sequencing (Read 1: 28 bp, Read 2: 120 bp). Read pairs (~345 million) were obtained with 100% valid UMIs, and 91.1% of them mapped onto the tiger puffer genome (assembly fTakRub1.2). Count data and the HE images were integrated using the Space Ranger pipeline (v1.1.0, 10X Genomics). Loupe Browser (v4.1.0, 10X Genomics) was used to export images and graphs of results from spatial transcriptomic analysis.

Cis-regulatory element prediction and plasmid preparation

A genomic sequence upstream of the translation start site was retrieved from the *Takifugu rubripes* fTakRub1.3 assembly for the *gnrh1* (NCBI: 101077516). Only *cebpd* and *crema* were expressed in the POA among the semilunar transcription factors. Therefore, we applied the Sequence Motif Location Tool (MoLoTool) to statistically identify the potential binding sites for cebpd and crema [42]. Then the obtained sequences were used to predict potential binding sites for cebpd (T[T/G]NNNNAA and TTNNNN[A/C]A) and crema (TGACGTCA) [43, 44]. To prepare the constructs for the luciferase assays, the coding sequence for *cebpd* (NCBI: 101064723) and a 702 bp fragment upstream of the grass puffer *gnrh1* translational start site (*gnrh1* WT) were synthesized *in vitro* by Genscript. The coding sequence for crema (NCBI: 101061679) was amplified by PCR. Both *cebpd* and *crema* sequences were cloned into the expression vector pcDNA3.1(+) between the *Nhe*I/*Apa*I sites, and *gnrh1* WT was inserted into the promoterless luciferase vector pGL4.15 between the *Sfi*I/*Hind*III sites. Mut1, mut2, and mut5 were generated by Genscript. Mut3 and mut4 were prepared using mut2 as the template with the traditional polymerase chain reaction (PCR) and subsequent cloning method. Primers for generating the mut3 and mut4 amplicons are listed in Table S3. pRL-CMV, used to monitor

669 transfection efficiency, was purchased from Promega.

670

671 **Dual-luciferase reporter assay**

672 Chinese hamster ovary (CHO) cells (ATCC CCL-61) were maintained in DMEM/Ham's
673 F-12 medium supplemented with 10% FBS at 37°C with 5% CO_2. Cells were seeded on
674 a 48-well plate at a density of 0.26×10^5 cells/well the day before transfection. A total of
675 250 ng of a plasmid mixture containing the *gnrh1* promoter luciferase construct, *cebpd* or
676 *crema* expression vector, and pRL-CMV at a ratio of 20:10:0.1 was prepared to transfect
677 the cells in each well using the jetPRIME transfection reagent (Polyplus). After 24 hours,
678 cells were harvested and luminescence was measured using a Dual-Luciferase Reporter
679 assay (Promega) and the SpectraMax i3 Multi-Mode Dectection Platform (Molecular
680 Devices). Promoter activation is presented as the relative luciferase activity, which is the
681 ratio of firefly (pGL4.15) to renilla (pRL-CMV) luminescence.

682

683 **Quantification and statistical analyses**

684 Results are presented as the means ± SEM. Two independent experiments were performed
685 for the Dual-Luciferase reporter assay and behavioral assay. Semilunar rhythmicity in the
686 expressions of semilunar genes was tested using the RAIN package [45] in R (Figure S2).
687 Where variance was significantly different between the groups, the Brown-Forsythe test
688 with Dunnett's T3 post hoc test was used (Figure 1E). Data with a normal distribution
689 were analyzed using one-way ANOVA with Dunnett's post hoc test (Figures 2B, 3G, 6B).
690 A two-tailed Welch's *t*-test was performed to calculate the *p*-values for the percentage
691 comparison of c-*fos* induction (Figure 4E) and the Dual-Luciferase reporter assay (Figure
692 6C).

Supplemental Table Legends

Table S1. Differentially expressed genes between individuals with a high and low GSI, related to Figure 2

Table S2. Differentially expressed genes between the spring tide and neap tide, related to Figure 2

Table S3. Primers for qPCR validation and generation of the gnrh1 mut3 and mut4 amplicons, related to Figure 6 and Figure S2

Supplemental Video Legends

Video S1. Trembling behavior during the beach-spawning, related to Figures 1 and 3

Video S2. Induction of trembling behavior by 10^{-11} M PGE_2, related to Figure 4

Video S3. Induction of trembling behavior by 10^{-8} M PGE_2, related to Figure 4

References

1 Andreatta, G., and Tessmar-Raible, K. (2020). The still dark side of the moon: Molecular mechanisms of lunar-controlled rhythms and clocks. J. Mol. Biol. *432*, 3525-3546.

2 Kaiser, T. S., and Neumann, J. (2021). Circalunar clocks-old experiments for a new era. Bioessays *43*, e2100074.

3 Levy, O., Appelbaum, L., Leggat, W., Gothlif, Y., Hayward, D. C., Miller, D. J., and Hoegh-Guldberg, O. (2007). Light-responsive cryptochromes from a simple multicellular animal, the coral Acropora millepora. Science *318*, 467-470.

4 Zurl, M., Poehn, B., Rieger, D., Krishnan, S., Rokvic, D., Veedin Rajan, V. B., Gerrard, E., Schlichting, M., Orel, L., Ćorić, A. et al. (2022). Two light sensors decode moonlight versus sunlight to adjust a plastic circadian/circalunidian clock to moon phase. Proc. Natl. Acad. Sci. U S A. *119*, e2115725119.

5 Kaiser, T. S., Poehn, B., Szkiba, D., Preussner, M., Sedlazeck, F. J., Zrim, A., Neumann, T., Nguyen, L. T., Betancourt, A. J., Hummel, T., et al. (2016). The genomic basis of circadian and circalunar timing adaptations in a midge. Nature *540*, 69-73.

6 Uno, Y. (1955). Spawning habit and early development of a puffer, *Fugu (Torafugu) niphobles* (Jordan et Snyder). J. Tokyo Univ. Fish. *42*, 169-183.

7 Martin, K. L. M., Van Winkle, R. C., Drais, J. E., and Lakisic, H. (2004). Beach-spawning fishes, terrestrial eggs, and air breathing. Physiol. Biochem. Zool. *77*, 750-759.

8 Nozaki, M., Tsutsumi, T., Kobayashi, H., Takei, Y., Ichikawa, T., Tsuneki, K., Miyagawa, K., Uemura, H., and Tatsumi Y. (1976). Spawning habit of the puffer, *Fugu niphobles* (Jordan et Snyder) I. Zool. Mag. *85*, 156-168.

9 Honma, Y., Ozawa, T., and Chiba, A. (1980). Maturation and spawning behavior of the puffer, *Fugu niphobles* occurring on the coast of Sado island in the sea of Japan (a preliminary report). Japan. J. Ichthyol. *27*, 129-138.

10 Motohashi, E., Yoshihara, T., Doi, H., and Ando, H. (2010). Aggregating behavior of the grass puffer, *Takifugu niphobles*, observed in aquarium during the spawning period. Zool. Sci. *27*, 559-564.

11 Ando, H., Shahjahan, M., and Hattori, A. (2013). Molecular neuroendocrine basis of lunar-related spawning in grass puffer. Gen. Comp. Endocrinol. *181*, 211-214.

12 Hamasaki, M., Takeuchi, Y., Miyaki, K., and Yoshizaki, G. (2013). Gonadal development and fertility of triploid grass puffer *Takifugu niphobles* induced by cold shock treatment. Mar. Biotechnol. (NY) *15*, 133-144.

13 Levavi-Sivan, B., Bogerd, J., Mañanós, E. L., Gómez, A., and Lareyre, J. J. (2010).

742 Perspectives on fish gonadotropins and their receptors. Gen. Comp. Endocrinol. *165*,
743 412-437.
744 14 Mazón, M. J., Molés, G., Rocha, A., Crespo, B., Lan-Chow-Wing, O., Espigares, F.,
745 Muñoz, I., Felip, A., Carrillo, M., Zanuy, S., et al. (2015). Gonadotropins in European
746 sea bass: Endocrine roles and biotechnological applications. Gen. Comp. Endocrinol.
747 *221*, 31-41.
748 15 Kobayashi, M., Sorensen, P. W., and Stacey, N. E. (2002). Hormonal and pheromonal
749 control of spawning behavior in the goldfish. Fish. Physiol. Biochem. *26*, 71–84.
750 16 Sorensen, P. W., and Wisenden, B.D. (2015). Fish pheromones and related cues. Wiley
751 Blackwell.
752 17 Yabuki, Y., Koide, T., Miyasaka, N., Wakisaka, N., Masuda, M., Ohkura, M., Nakai,
753 J., Tsuge, K., Tsuchiya, S., Sugimoto, Y., et al. (2016). Olfactory receptor for
754 prostaglandin $F_{2\alpha}$ mediates male fish courtship behavior. Nat. Neurosci. *19*, 897-904.
755 18 Sorensen, P. W. (2013). Behavioral analysis of pheromone in fish. Methods Mol. Biol.
756 *1068*, 293-305.
757 19 Yamahira, K. (1997). Proximate factors influencing spawning site specificity of the
758 puffer fish Takifugu niphobles. Mar. Ecol. Prog. Ser. *147*, 11-19.
759 20 Yamamoto, M., and Ueda, K. (1979). Comparative morphology of fish olfactory
760 epithelium. IX. Tetraodontiformes. Zool. Mag. *88*, 210-218.
761 21 Ståhl, P. L. Salmén, F., Vickovic, S., Lundmark, A., Navarro, J. F., Magnusson, J.,
762 Giacomello, S., Asp, M., Westholm, J.O., Huss, M., et al. (2016). Visualization and
763 analysis of gene expression in tissue sections by spatial transcriptomics. Science *353*,
764 78-82.
765 22 Pandolfi, M., Pozzi, A. G., Cánepa, M., Vissio, P. G., Shimizu, A., Maggese, M. C.,
766 and Lobo, G. (2009). Presence of beta-follicle-stimulating hormone and beta-
767 luteinizing hormone transcripts in the brain of *Cichlasoma dimerus* (Perciformes:
768 Cichlidae): effect of brain-derived gonadotropins on pituitary hormone release.
769 Neuroendocrinology *89*, 27-37.
770 23 Elisio, M., Soria, F. N., Fernandino, J. I., Strüssmann, C. A., Somoza, G. M., and
771 Miranda, L. A. (2012). Extrahypophyseal expression of gonadotropin subunits in
772 pejerrey *Odontesthes bonariensis* and effects of high water temperatures on their
773 expression. Gen. Comp. Endocrinol. 175, 329-336
774 24 So, W. K., Kwok, H. F., and Ge, W. (2005). Zebrafish gonadotropins and their
775 receptors: II. Cloning and characterization of zebrafish follicle-stimulating hormone
776 and luteinizing hormone subunits--their spatial-temporal expression patterns and
777 receptor specificity. Biol. Reprod. *72*, 1382-1396.

778 25 Ogawa, S., Yamamoto, N., Hagio, H., Oka, Y., and Parhar, I. S. (2022). Multiple
779 gonadotropin-releasing hormone systems in non-mammalian vertebrates: Ontogeny,
780 anatomy, and physiology. J. Neuroendocrinol. *34*, e13068.
781 26 Sinclair, A. R. E. (1977). Lunar cycle and timing of mating season in Serengeti
782 wildebeest. Nature *267*, 832-833.
783 27 Yonezawa, T., Uchida, M., Tomioka, M., and Matsuki, N. (2016). Lunar cycle
784 influences spontaneous delivery in cows. PLoS One *11*, e0161735n.
785 28 Casiraghi, L., Spiousas, I., Dunster, G. P., McGlothlen, K., Fernández-Duque, E.,
786 Valeggia, C., and de la Iglesia, H. O. (2021). Moonstruck sleep: Synchronization of
787 human sleep with the moon cycle under field conditions. Sci. Adv. *7*, eabe0465.
788 29 Helfrich-Förster, C, Monecke, S., Spiousas, I., Hovestadt, T., Mitesser, O., and Wehr,
789 T. A. (2021). Women temporarily synchronize their menstrual cycles with the
790 luminance and gravimetric cycles of the Moon. Sci. Adv. *7*, eabe1358.
791 30 Wehr, T. A., and Helfrich-Förster, C. (2021). Longitudinal observations call into
792 question the scientific consensus that humans are unaffected by lunar cycles.
793 Bioessays *43*, e2100054.
794 31 Balamurugan, K., and Sterneck, E. (2013). The many faces of C/EBPδ and their
795 relevance for inflammation and cancer. Int. J. Biol. Sci. *9*, 917-933.
796 32 Chen, Y., Chen, Y., Shi, C., Huang, Z., Zhang, Y., Li, S., Li, Y., Ye, J., Yu, C., Li, Z. et
797 al. (2018). SOAPnuke: a MapReduce acceleration-supported software for integrated
798 quality control and preprocessing of high-throughput sequencing data. Gigascience *7*,
799 1-6.
800 33 Kim, D., Langmead, B., and Salzberg, S.L. (2015). HISAT: a fast spliced aligner with
801 low memory requirements. Nat. Methods *12*, 357-360.
802 34 Pertea, M., Pertea, G. M., Antonescu, C. M., Chang, T. C, Mendell, J. T., and Salzberg,
803 S. L. (2015). StringTie enables improved reconstruction of a transcriptome from
804 RNA-seq reads. Nat. Biotechnol. *33*, 290-295.
805 35 Trapnell, C., Roberts, A., Goff, L., Pertea, G., Kim, D., Kelley, D. R., Pimentel, H.,
806 Salzberg, S. L., Rinn, J. L., and Pachter L. (2012). Differential gene and transcript
807 expression analysis of RNA-seq experiments with TopHat and Cufflinks. Nat. Protoc.
808 *7*, 562-578.
809 36 Kong, L., Zhang, Y., Ye, Z. Q., Liu, X. Q., Zhao, S. Q., Wei, L., and Gao, G. (2007).
810 CPC: assess the protein-coding potential of transcripts using sequence features and
811 support vector machine. Nucleic Acids Res. *35*, W345-W349.
812 37 Langmead, B., and Salzberg, S. L. (2012). Fast gapped-read alignment with Bowtie
813 2. Nat. Methods *9*, 357-359.

38 Li, B., and Dewey, C. N. (2011). RSEM: accurate transcript quantification from RNA-Seq data with or without a reference genome. BMC Bioinformatics *12*, 323.
39 Love, M. I., Huber, W., and Anders, S. (2014). Moderated estimation of fold change and dispersion for RNA-seq data with DESeq2. Genome Biol. *15*, 550.
40 Buchfink, B., Xie, C., and Huson, D. H. (2015). Fast and sensitive protein alignment using DIAMOND. Nat. Methods *12*, 59-60.
41 Schindelin, J. Arganda-Carreras, I., Frise, E., Kaynig, V., Longair, M., Pietzsch, T., Preibisch, S., Rueden, C., Saalfeld, S., Schmid, B., et al. (2012). Fiji: an open-source platform for biological-image analysis. Nat. Methods *9*, 676–682.
42 Kulakovskiy, I. V., Vorontsov, I. E., Yevshin, I. S., Sharipov, R. N., Fedorova, A. D., Rumynskiy, E. I., Medvedeva, Y. A., Magana-Mora, A., Bajic, V. B., Papatsenko, D. A., et al. (2018). HOCOMOCO: towards a complete collection of transcription factor binding models for human and mouse via large-scale ChIP-Seq analysis. Nucleic Acids Res. *46*, D252-D259.
43 Wang, Q., Ozer, H. G., Wang, B., Zhang, M., Urabe, G., Huang, Y., Kent, K. C., and Guo, L.W. (2021). A hierarchical and collaborative BRD4/CEBPD partnership governs vascular smooth muscle cell inflammation. Mol. Ther. Methods Clin. Dev. *21*, 54-66.
44 Loeken, M. R. (1993). Effects of mutation of the CREB binding site of the somatostatin promoter on cyclic AMP responsiveness in CV-1 cells. Gene Expr. *3*, 253-264.
45 Thaben, P. F., and Westermark, P. O. (2014). Detecting rhythms in time series with RAIN. J. Biol. Rhythms *29*, 391-400.

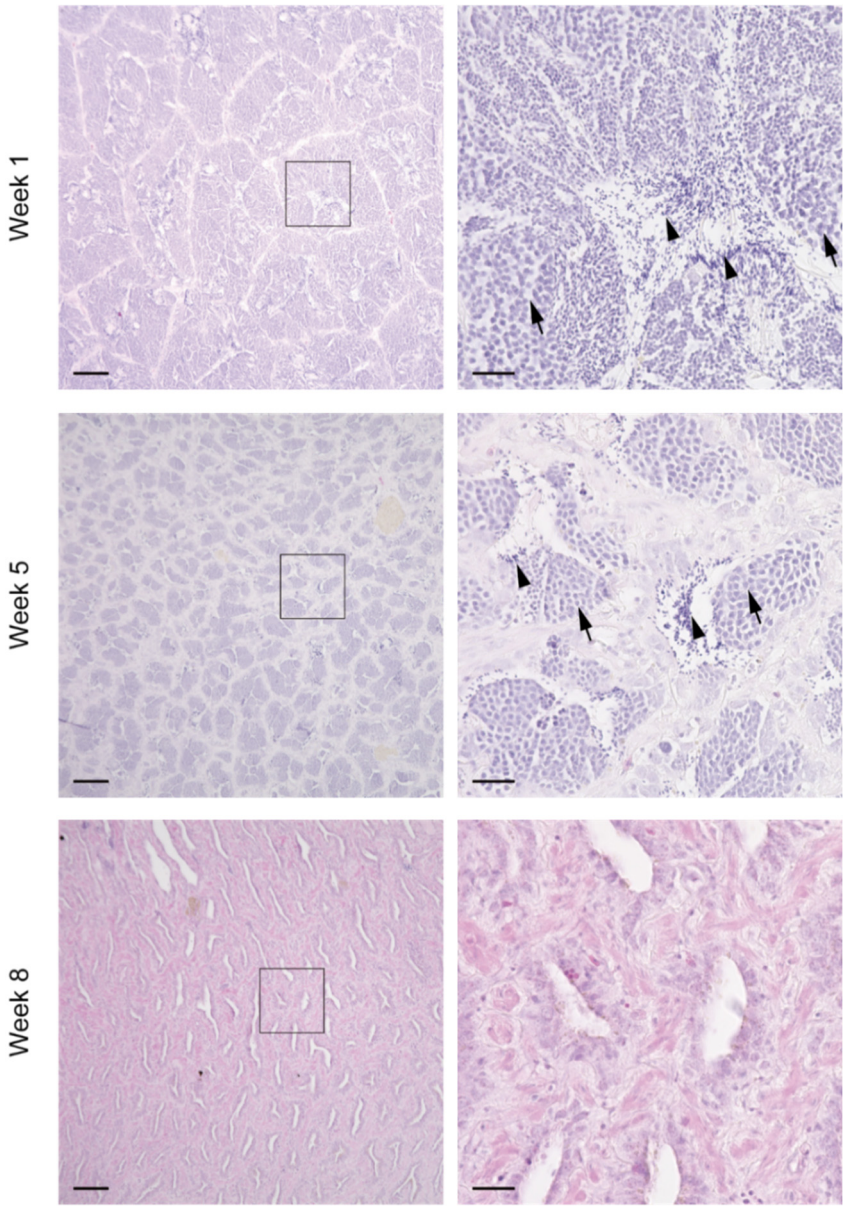

Figure S1. Changes in testicular morphology during the breeding season, related to Figure 1

Arrow and arrowhead indicate spermatocytes and spermatids, respectively. A marked reduction of in the number of spermatocytes and spermatids was observed over the course of the breeding season. Scale bars: 100 μm (left), 20 μm (right).

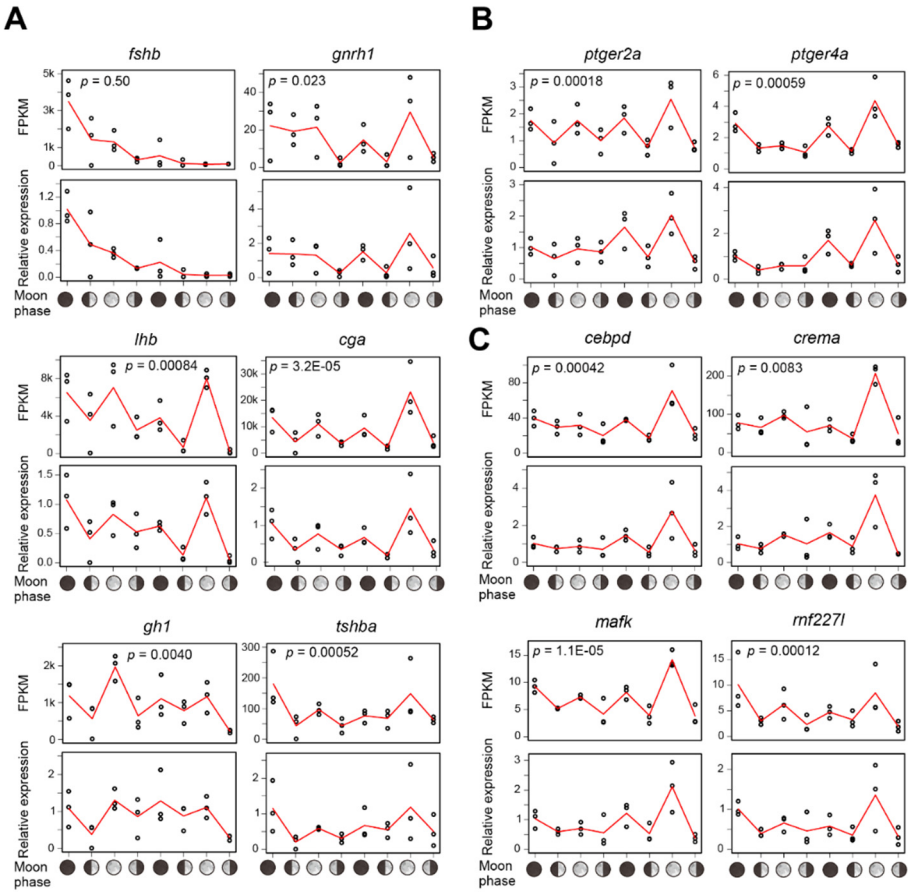

Figure S2. Independent verification of RNA-seq quantification, related to Figures 2 and 5

(A) qPCR validations of gene expressions for the same RNA samples that were used for the RNA-seq analysis for *fshb* and the five semilunar hormone genes (*gnrh1*, *lhb*, *cga*, *gh1*, and *tshba*). Red lines represent the means, and individual values are shown using open circles (n = 3). *P*-values for semilunar rhythmicity were tested using the RAIN package in R.

(B) qPCR validations of gene expressions for the same RNA samples that were used for the RNA-seq analysis for semilunar receptor genes for pheromone (*ptger2a* and *ptger4a*). Red lines represent the means, and individual values are shown using open circles (n = 3). *P*-values for semilunar rhythmicity were tested using the RAIN package in R.

(C) qPCR validations of gene expressions for the same RNA samples that were used for the RNA-seq analysis for semilunar transcription factors (*cebpd*, *crema*, *mafk*, and *rnf227l*). Red lines represent the means, and individual values are shown using open circles (n = 3). *P*-values for semilunar rhythmicity were tested using the RAIN package in R.

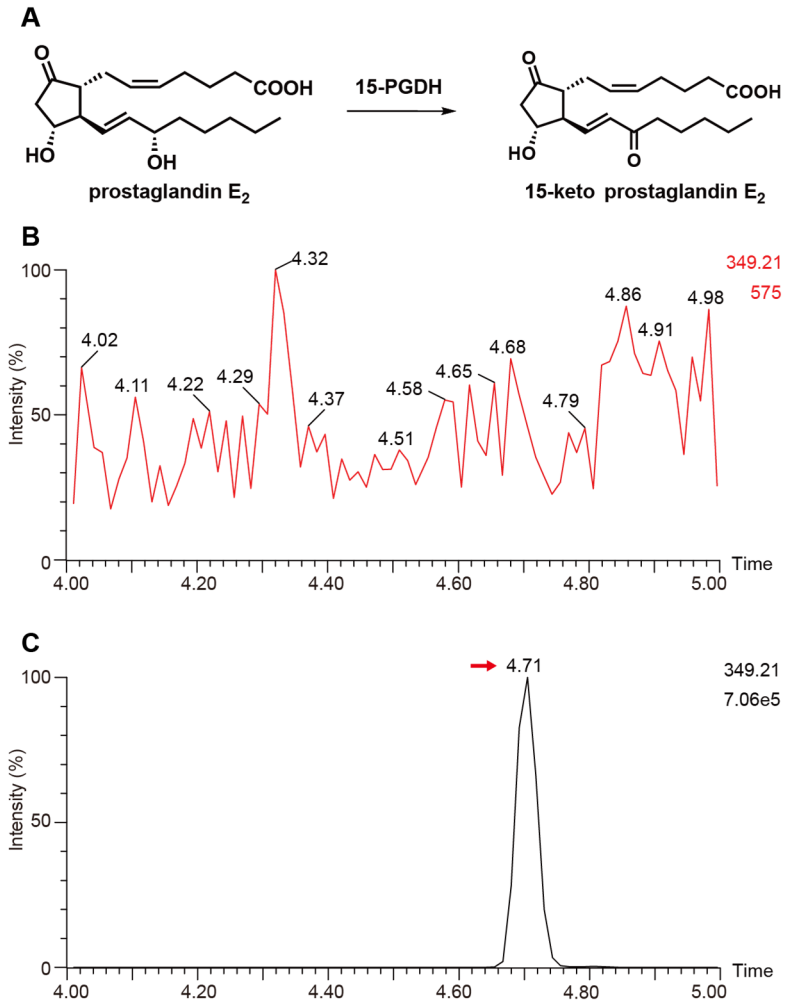

Figure S3. 15-keto-PGE$_2$ was not detected in the seawater during beach-spawning, related to Figure 3

(A) Prostaglandin E$_2$ (PGE$_2$) metabolism by 15-hydroxyprostaglandin dehydrogenase (15-PGDH).

(B) Mass chromatogram targeting 15-keto-PGE$_2$ (*m/z* 349.21) in the seawater at 0 m.

(C) Mass chromatogram for the authentic 15-keto-PGE$_2$ (100 nM in 50% aqueous MeOH). The red arrow indicates the peak of 15-keto-PGE$_2$.

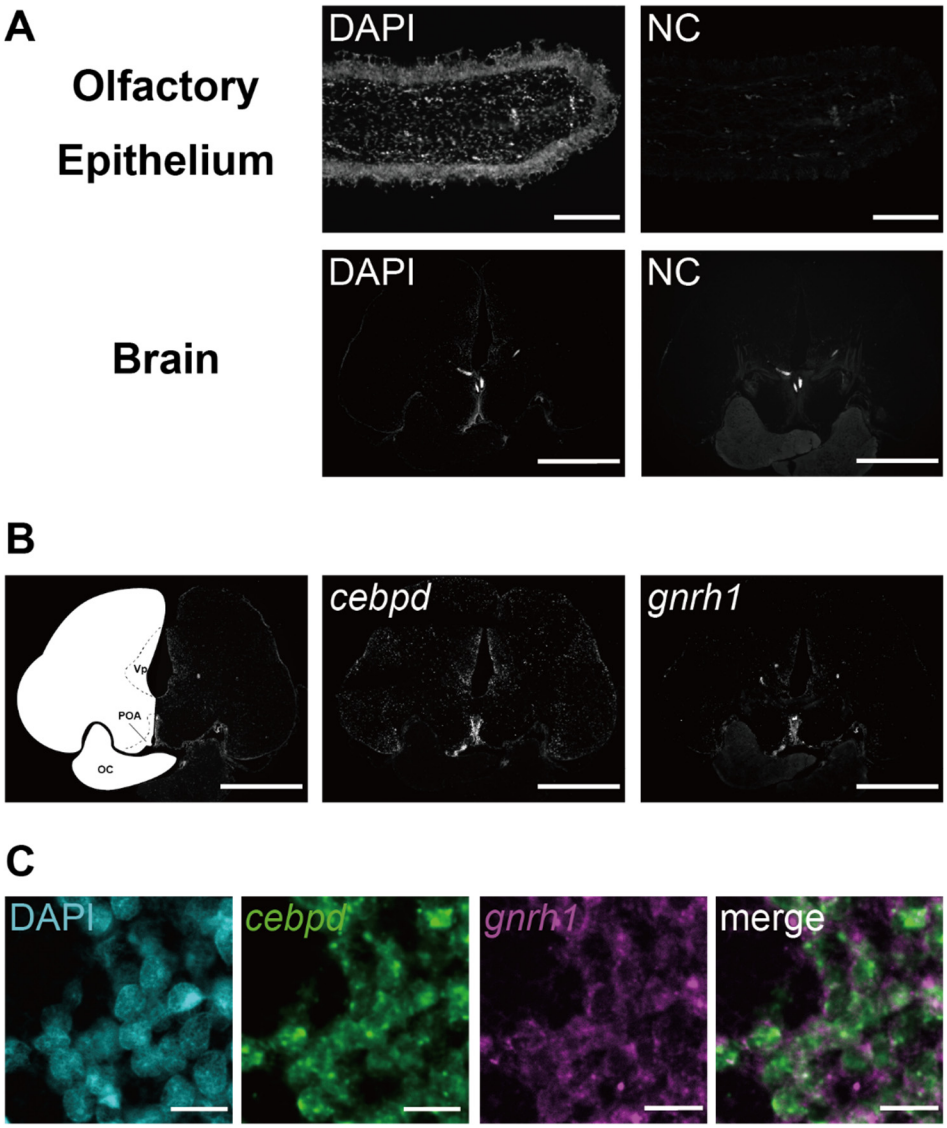

Figure S4. Results of multiplex fluorescent in situ hybridization, related to Figures 4 and 6

(A) Overview of the negative control (NC) slides for the olfactory epithelium and the brain. These slides were stained with DAPI and a negative control probe against the bacterial *DapB* gene. Intense fluorescence observed in the center of the brain section represents blood vessels due to autofluorescence of blood cells. Scale bar: 100 μm for olfactory epithelium, and 1 mm for brain.

(B) Low magnification view of Figure 6D. Left) DAPI image on the right and brain atlas on the left; Center) *cebpd*; Right) *gnrh1*. Scale bar: 1 mm.

(C) Boxed areas in Figure 6D are shown at a higher magnification. Scale bar: 10 μm.

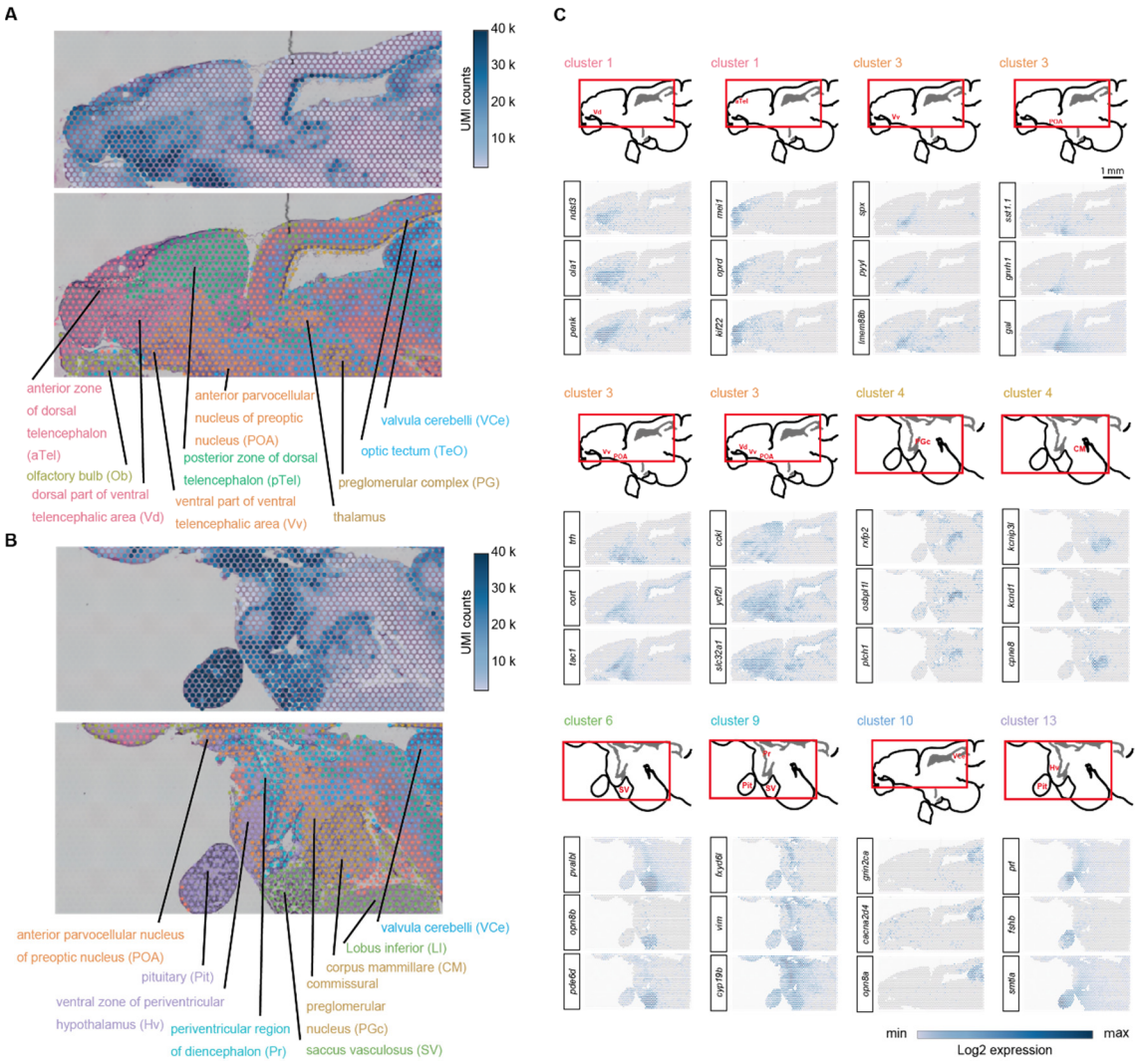

Figure S5. Spatially resolved expression and clustering in the puffer brain, related to Figure 5

(A and B) Dorsal (A) and ventral (B) sagittal puffer brain sections were stained using HE. Image overlays containing data for UMI counts for total genes (top) and spatial clustering based on total differentially expressed genes (bottom) are shown. (C) Expression of marker genes for each cluster.

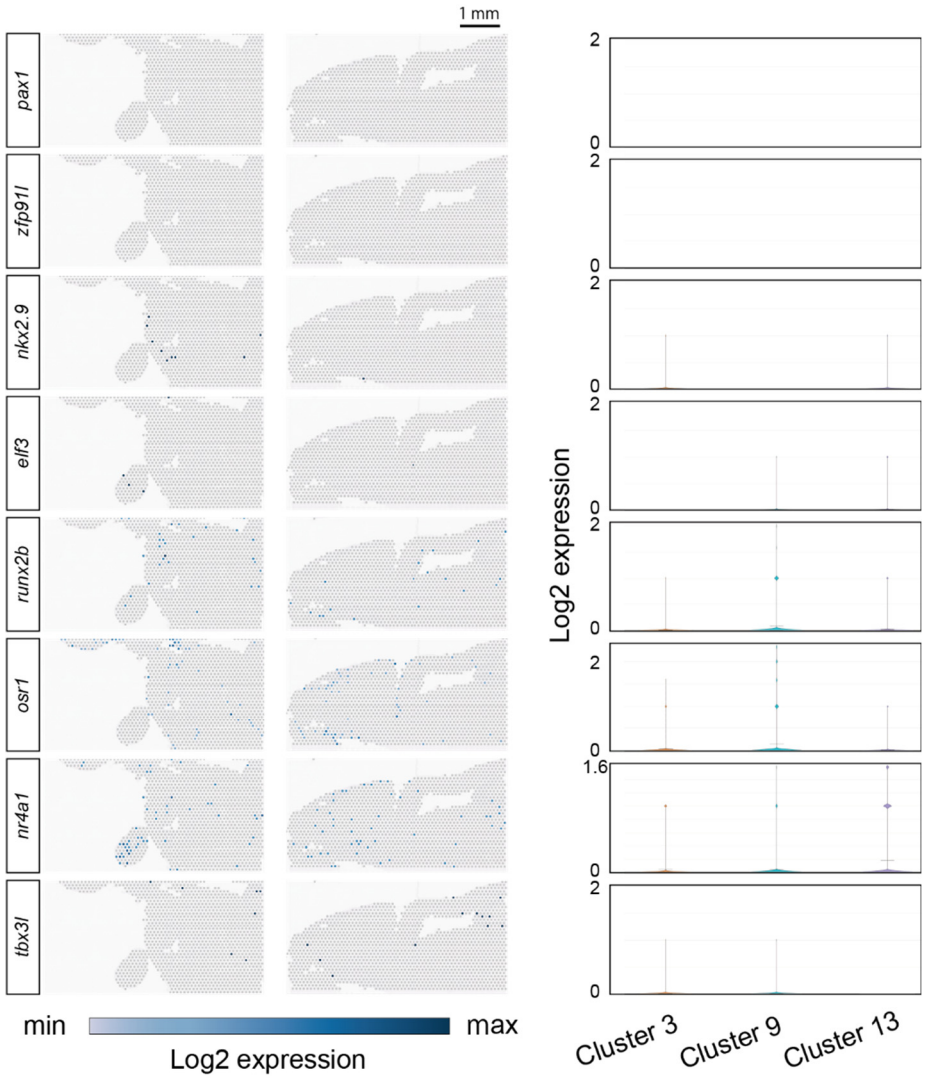

Figure S6. Expression of semilunar transcription factors that did not overlap with the semilunar hormone genes, related to Figure 5.

Left and right panels show the spatial expression and violin plot for semilunar transcription factors, respectively. Expression of these transcription factors did not overlap with semilunar hormone genes.

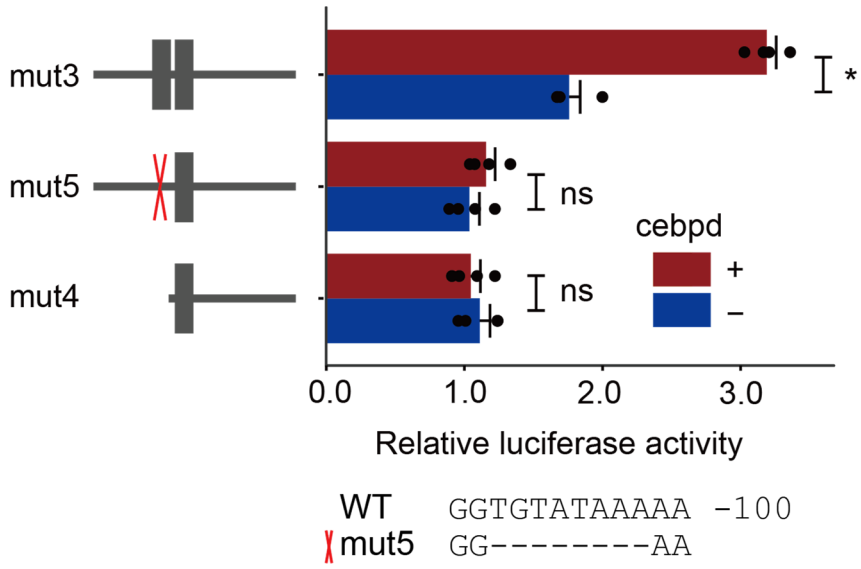

Figure S7. Mutation in the cebpd binding site reduces cebpd-induced promoter activity of grass puffer *gnrh1*, related to Figure 6.

Mutant reporters fused to the luciferase gene were assayed for their activities with or without *cebpd* co-transfection. Each value represents the mean + SEM for a single assay (Welch's t-test, $t_{(5.838)}$ = 13.58 [mut3], $t_{(5.940)}$ = 1.226 [mut4], $t_{(5.967)}$ = 0.6310 [mut5], *p < 0.0001, n = 4).